

Mechanism of Ser88 Phosphorylation-Induced Dimer Dissociation in Dynein Light Chain LC8

Fei Xiao,[†] Jingwei Weng,[†] Kangnian Fan,[†] and Wenning Wang^{*,†,‡}

Shanghai Key Laboratory of Molecular Catalysis and Innovative Materials, Department of Chemistry, and Institute of Biomedical Sciences, Fudan University, Shanghai 200433, People's Republic of China

Received: May 27, 2010; Revised Manuscript Received: October 17, 2010

Dynein light chain LC8 is a highly conserved, dimeric protein involved in a variety of essential cellular events. Phosphorylation at Ser88 was found to promote mammalian cell survival and regulate the dimer to monomer transition at physiological pH. Combining molecular dynamics (MD) simulation and free energy calculation methods, we explored the atomistic mechanism of the phosphorylation-induced dimer dissociation. The MD simulation revealed that phosphorylation/phosphomimetic mutation at Ser88 opens an entrance into the dimer interface for water molecules, which disturb the hydrogen bond network around His55 and is expected to raise the pK_a value and protonation ratio of His55 as well. The free energy calculations showed that the S88E mutation destabilized the dimer by 6.6 kcal/mol, in good agreement with the experimental value of 8.1 kcal/mol. The calculated destabilization upon phosphorylation is 50.8 kcal/mol, showing that phosphorylation definitely prevents dimer formation under physiological conditions. Further analysis of the calculated free energy changes demonstrated that the electrostatic contribution dominates the impact of phosphorylation on dimer dissociation.

1. Introduction

Dynein light chain LC8 (also known as DYNLL1, DLC8, and PIN) was first identified as a light chain of the outer arm of *Chlamydomonas* axonemal dynein.¹ It was subsequently shown to be an essential component of the cytoplasmic dynein complexes^{2–5} and actin-based motor myosin V⁶ and was revealed to associate with the dynein complex through its interaction with dynein intermediate chain (IC).^{7,8} In addition to being an essential component of the motor complex, LC8 binds to a large number of proteins with diverse biological functions.⁹ For example, LC8 associates with and inhibits the activity of neuronal nitric oxide synthase,¹⁰ giving rise to its alternative designation as PIN (protein inhibitor of neuronal nitric oxide synthase). It also binds to IκBα,¹¹ an inhibitor of NF-κB⁴, to Bim (Bcl-2-interacting mediator of cell death) and Bmf (Bcl-2-modifying factor),¹² both of which are proapoptotic members of the Bcl-2 family of proteins, to p21-activated kinase 1,¹³ and to p53-binding protein 1.¹⁴

LC8 is a highly conserved protein consisting of 89 amino acids¹⁵ and exists as a homodimer under neutral pH conditions.^{4,16–18} Structural studies of LC8 showed that the two monomers assemble into a domain-swapped dimer by exchanging the β 2-strands to form an antiparallel β -sheet across the dimer interface^{16,17} (Figure 1a), at the clefts of which there are also two identical ligand binding sites. The LC8 dimer was found to dissociate in a pH-dependent manner, in which the monomeric population increases with the decrease of the pH value.^{18,19} The overall structure of the monomeric LC8 is similar to that of the dimer form except for the β 2-strand, but the ligand binding is disrupted upon dimer dissociation.^{20,21}

Recently, it was reported that the dimer dissociation of LC8 can also be regulated at physiological condition through phosphorylation at Ser88.²² Initially, LC8 was found to be the phosphorylation substrate of Pak1, and Ser88 phosphorylation can promote the

survival and anchorage-independent growth of breast cancer.^{13,22} Subsequent structural and biochemical studies demonstrated that Pak1 can directly bind to LC8 but questioned the role of Pak1 as the phosphorylation kinase of LC8.²³ Although the upstream regulator of LC8 is still unclear, it is certain that LC8 is phosphorylated in vivo. Moreover, the biochemical studies clearly showed that phosphorylation at Ser88 can disrupt the ligand binding as well as dimer assembly.^{22,24} This implicates a regulatory role for Ser88 phosphorylation of potential functional importance. A recent NMR study of the phosphomimetic S88E mutant of LC8 revealed that the S88E mutation raises the dimer dissociation constant (K_D) through both a higher k_{off} and lower k_{on} and gave a quantitative estimation of the impact of phosphomimetic mutation on dimer dissociation.²⁵

In this study, we combined MD simulations and free energy calculations to explore the atomic details and energetics of the phosphorylation-induced LC8 dimer dissociation. Molecular dynamics (MD) simulation of biomolecules provides detailed atomistic information that is often difficult to obtain directly from experiments. The MD simulation trajectories revealed that phosphorylation at Ser88 opens an entrance into the dimer interface for water molecules, which disturb the H-bond network around His55 and may change the protonation state of His55 and thereby promote the dimer dissociation. The results of the free energy calculation agree with the experimental study of the S88E mutant and provide the energetics of the phosphorylation-induced dimer dissociation.

2. Methods

2.1. Molecular Dynamics Simulations. All simulations were performed using NAMD 2.6²⁶ and the CHARMM27 force field.²⁷ Initial coordinates of the protein were taken from its crystal structure¹⁶ (PDB entry 1CMI) and solvated in a TIP3P²⁸ water box. The temperature and the pressure were maintained at 300 K and 1 atm by Langevin dynamics and the Nosé–Hoover Langevin piston method, respectively.^{29,30} The non-bonded interactions were truncated at a distance of 12 Å and smoothed by a switching function since 10 Å. The particle-

* Corresponding author. Fax: 86-21-65641740; e-mail: wnwang@fudan.edu.cn.

[†] Department of Chemistry.

[‡] Institute of Biomedical Sciences.

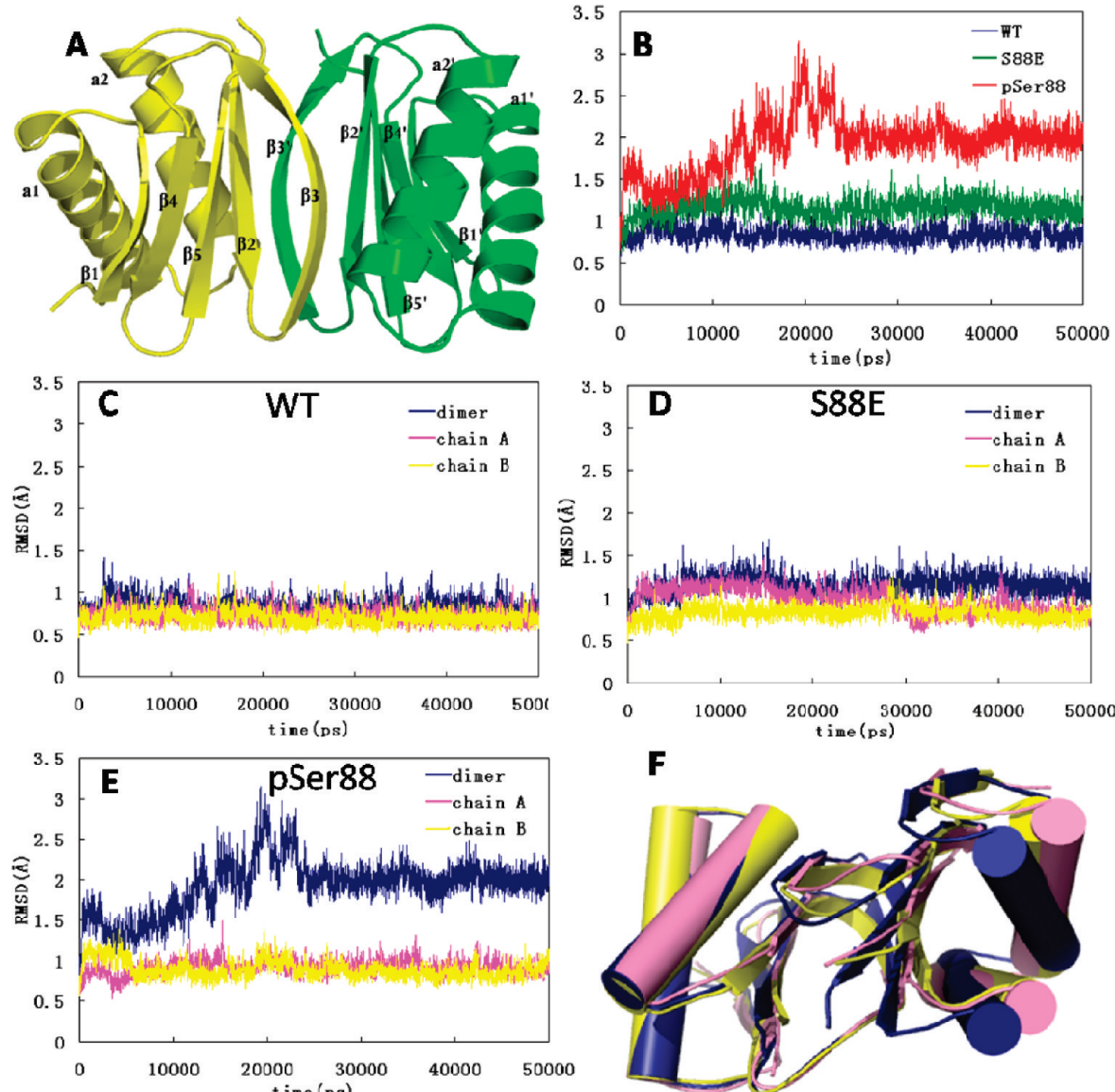


Figure 1. (A) A ribbon diagram of crystal structure of the LC8 dimer (PDB code 1CM1).¹⁶ The 13-residue nNOS peptides are not shown. (B) Root mean-square-deviation (rmsd) of the C_α atoms with respect to their starting structures along the 50 ns MD simulation trajectories for WT (blue), S88E (green), and pSer88 LC8 (red), respectively. rmsd of C_α atoms of monomers (yellow and purple) in comparison with those of dimers (dark blue) for WT (C), S88E (D), and pSer88 (E) are shown, respectively. (F) Comparison of the structures at the end of 50 ns simulations of WT (dark blue), S88E (pink), and pSer88 (yellow) LC8. Superposition is made against one monomer of LC8.

mesh Ewald (PME) method^{31,32} was employed to compute electrostatic interactions. All the bonds between hydrogen and the atom to which it is bonded were kept rigid using the SHAKE algorithm,³³ and a time step of 2 fs was used. The system was initially energy minimized for 1000 steps and equilibrated for five states of 20 ps each. Then the heavy atoms were harmonically constrained with a spring force constant of 70 kcal/mol/Å² for 20 ps. The force constant was reduced to 35 and then to 10 kcal/mol/Å². Only α -carbon atoms were constrained afterward with a force constant of 1 kcal/mol/Å². Finally, all the constraints were removed and a 50 ns production run was performed.

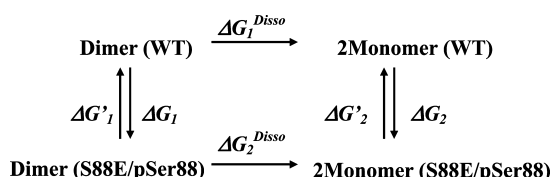
2.2. Steered Molecular Dynamics Simulations. Steered molecular dynamics (SMD) simulation was used to accelerate the process of dimer dissociation. External forces of opposite directions are applied to all $C\alpha$ atoms of the two monomers parallel to the line connecting their mass centers to accelerate the dimer dissociation. The potential form used can be expressed as:

$$V = k[D_{MC}(t) - D_{MC}^*(t)]^2 \quad (1)$$

in which $D_{MC}(t)$ is the instantaneous distance between the mass centers of the two monomers and is forced to follow the variation of the reference value $D_{MC}^*(t)$ which was set to increase linearly with a constant velocity of 0.02 Å/ps. The force constant k was set to 3 kcal/mol/Å². The Tcl force interface of NAMD was used in the SMD simulations.

2.3. Free Energy Calculations. The free energy changes due to the S88E mutation and phosphorylation at Ser88 were calculated from the thermodynamics cycle shown in Scheme 1. The dual topology method³⁴ was employed to perform the “alchemical transformation”. Transformations in dimeric and monomeric LC8 were performed using the free energy perturbation (FEP) method,³⁵ in which the Hamiltonian is made as a function of a coupling parameter λ that varies progressively from 0 to 1 corresponding to N nonphysical intermediates connecting the two thermodynamic states (i.e., wild type and mutated/

SCHEME 1: Thermodynamic Cycle Used To Calculate the Difference of Dimer Dissociation Free Energy Change between Wild Type and S88E/pSer88 LC8 (see text for more details)



phosphorylated states). The free energy difference between the two states can be expressed as eq 2:

$$\Delta G_{a \rightarrow b} = G(\lambda_b) - G(\lambda_a) = -k_B T \sum_{k=1}^N \ln \left\langle \exp \left[-\frac{U(x, \lambda_{k+1}) - U(x, \lambda_k)}{k_B T} \right] \right\rangle_{\lambda_k} \quad (2)$$

where k_B is the Boltzmann constant, T is the temperature, and $U(x; \lambda_k)$ is the potential energy of the system that is dependent on the Cartesian coordinates and the coupling parameter λ_k . In the course of the alchemical transformations, the reaction paths were divided into 131 and 67 windows in the dimer and monomer systems, respectively, with uneven widths of $\lambda = 0$ to 1. Narrower windows were defined toward the end points of the simulation to avoid singularities. Each window involved 80 or 150 ps of equilibration in monomer or dimer systems, respectively, followed by 100 ps of data collection, summing to a total of 11 or 24 ns simulations. The absolute free energy of mutation involves the alchemy transformations of both a side chain (neutral to negatively charged) and a sodium counterion (the charge of which from 0 to +1) in order to maintain the overall charge of the system being zero throughout the transformation. Assuming that each free energy difference computed at a given λ_k -state constitutes an independent observable, the error was determined using a first-order approximation, in which the change in the Gibbs free energy between two intermediate states is expressed as:

$$\Delta G = -k_B T \left\{ \ln \left\langle \exp \left[-\frac{1}{k_B T} \Delta U(x, \lambda_k) \right] \right\rangle_{\lambda_k} \pm \frac{\delta \varepsilon}{\left\langle \exp \left[-\frac{1}{k_B T} \Delta U(x, \lambda_k) \right] \right\rangle_{\lambda_k}} \right\} \quad (3)$$

$\delta \varepsilon$ is the statistical error of the ensemble average, $\langle \exp [-(1/k_B T) \Delta U(x, \lambda_k)] \rangle$, defined as:

$$\delta \varepsilon^2 = \frac{1 + 2\tau}{N} \left\{ \left\langle \exp \left[-\frac{2}{k_B T} \Delta U(x, \lambda_k) \right] \right\rangle_{\lambda_k} - \left\langle \exp \left[-\frac{1}{k_B T} \Delta U(x, \lambda_k) \right] \right\rangle_{\lambda_k}^2 \right\} \quad (4)$$

where N is the number of the samples accrued in the free energy calculation, and $(1 + 2\tau)$ is the sampling ratio of the latter.

In order to interpret the free energy changes in terms of physically meaningful contributions, we proximately decomposed the free energy differences into electrostatic and van der

Waals terms $\Delta G_{a \rightarrow b}^{\text{elec}}$ and $\Delta G_{a \rightarrow b}^{\text{vdW}}$, which are expressed as eqs 3 and 4.

$$\Delta G_{a \rightarrow b}^{\text{elec}} = -k_B T \sum_{k=1}^N \ln \left\langle \exp \left[-\frac{U^{\text{elec}}(x, \lambda_{k+1}) - U^{\text{elec}}(x, \lambda_k)}{k_B T} \right] \right\rangle_{\lambda_k} \quad (5)$$

$$\Delta G_{a \rightarrow b}^{\text{vdW}} = -k_B T \sum_{k=1}^N \ln \left\langle \exp \left[-\frac{U^{\text{vdW}}(x, \lambda_{k+1}) - U^{\text{vdW}}(x, \lambda_k)}{k_B T} \right] \right\rangle_{\lambda_k} \quad (6)$$

in which U^{elec} and U^{vdW} are the electrostatic and van der Waals potential energy of the system, respectively.

3. Results

3.1. Conventional Molecular Dynamics Simulations. Fifty-nanosecond conventional MD simulations were carried out in wild-type, S88E, and phosphorylated LC8 (pSer88) systems, respectively. The time series of the root-mean-square deviation (rmsd) values of C_α atoms along the trajectories showed that the backbone conformation of the wild type protein is very stable, while the point mutation or phosphorylation of Ser88 evidently results in the increase of rmsd values (Figure 1b). For the pSer88 system, the rmsd value obviously increased in the first 20 ns and kept stable during the last 25 ns of the simulation. We further compared the rmsd values of the dimeric and monomeric LC8 along the trajectories. For the wild type protein, there is hardly any difference between the rmsd values of dimer and monomer, indicating the stability of the dimeric conformation (Figure 1c). In both S88E and pSer88 systems, the mutation and phosphorylation of Ser88 induced little perturbation on the backbone conformation of each monomer (C_α rmsd around 0.8 Å for WT, 0.9 Å for S88E, and 1.1 Å for pSer88), but the rmsd values of the dimer are larger than those of the monomers, especially in the case of pSer88 (Figure 1d and 1e), indicating the interdomain conformational change. Comparing the end structures of the 50 ns MD simulations of the three systems by superimposing one of the monomers revealed that the perturbation on Ser88 changes the relative positions of the two monomers (Figure 1f). With respect to the wild type protein, the two monomers were moving away from each other at the C-terminal end around Ser88, although the magnitude of this conformational change is small.

The separation at the C-terminus is directly reflected by the distance between the two Ser88 residues of each monomer. In the wild type protein, the distance between the C_α atoms of Ser88 and Ser88' (Ser88' denotes the residue on the other monomer) remained stable at the value of 6.6 Å throughout the simulation. For the other two systems, the C_α distances between E88/E88' or pS88/pS88' fluctuated around 8.8 and 11.7 Å in the last 20 ns of the simulations, respectively. Detailed inspection revealed that the mutation/phosphorylation disrupted the hydrogen bond between the side chains of Ser88 and Ser88' and the negatively charged E88/E88' and pS88/pS88' are expected to induce like-charge repulsion between the two residues, both of which resulted in the increased distance between the C-terminus of the two monomers. In the crystal structure of LC8/Swa³⁶ and LC8_{S88E}/Swa²⁵ complexes, the C_α distances between Ser88/E88 and Ser88'/E88' are 6.1 and 6.5 Å, respectively. It was shown that the binding of Swa can shift the dimer–monomer equilibrium toward the dimer.²⁴ Therefore, the small structural difference between the wild type protein

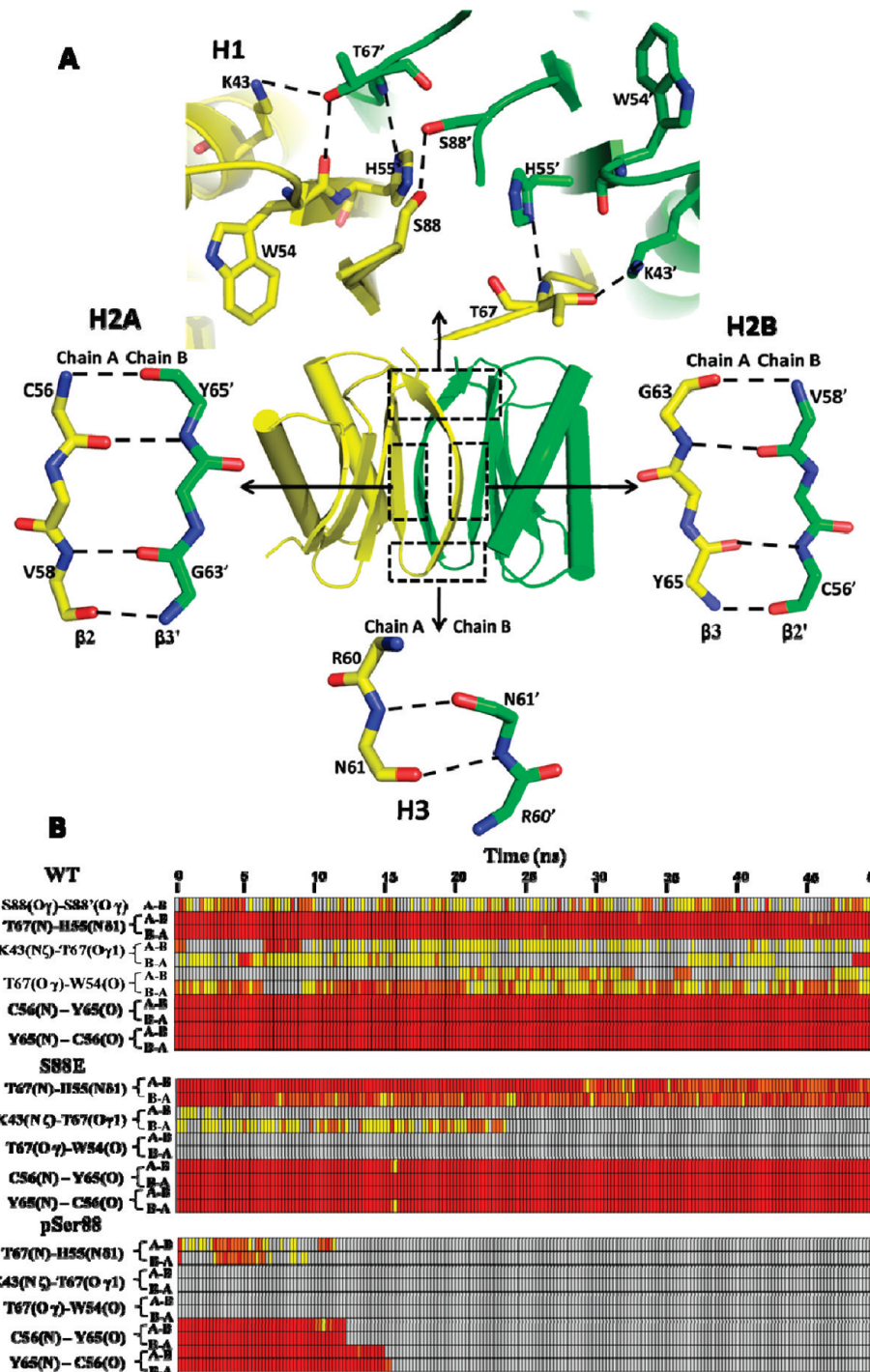


Figure 2. Hydrogen bond network at the dimer interface of LC8. (A) Illustration of the three groups of hydrogen bonds across the dimer interface. (B) Variation of some interdomain hydrogen bonds along the 50 ns MD simulation trajectories of WT, S88E, and pSer88 LC8. Each grid represents 250 ps, and its color corresponds to the percentage of hydrogen bond emergence in this period (red: $\geq 60\%$, orange: 40%, yellow: 20%, and gray: none). The hydrogen bond cutoffs are set by the donor–acceptor distance less than 3.5 Å and the deviation of the donor–hydrogen–acceptor angle less than 30° from 180°.

and the S88E mutant may be attributed to the ligand binding. The binding of the Swa peptide may hinder the tendency of S88E to dissociate.

Across the dimer interface of LC8, there is a hydrogen bond network that associates the two monomers. According to their location at the interface, these hydrogen bonds can be divided into three groups: **H1**, **H2**, and **H3** (Figure 2a). Hydrogen bonds in the **H1** group mainly distribute around the C-termini, including side-chain hydrogen bonds between Ser88–Ser88' (in WT only), Thr67–His55', Thr67–Lys43', and Thr67–Trp54'.

The **H2** group hydrogen bonds locate at the middle of the dimer interface including main-chain hydrogen bond pairs between Tyr65–Cys56' and Val58–Gly63'. The **H3** group locates at the opposite side of **H1**, containing a pair of main-chain hydrogen bonds between Asn61 and Asn61' (Figure 2a). In the wild type LC8, most of these hydrogen bond interactions were stable throughout the 50 ns simulation. For S88E and pSer88 LC8, however, the hydrogen bonds of group **H1** were disturbed. The H-bonds pairs between Thr67–His55' were severely impaired in S88E and totally disrupted in pSer88 LC8, and the

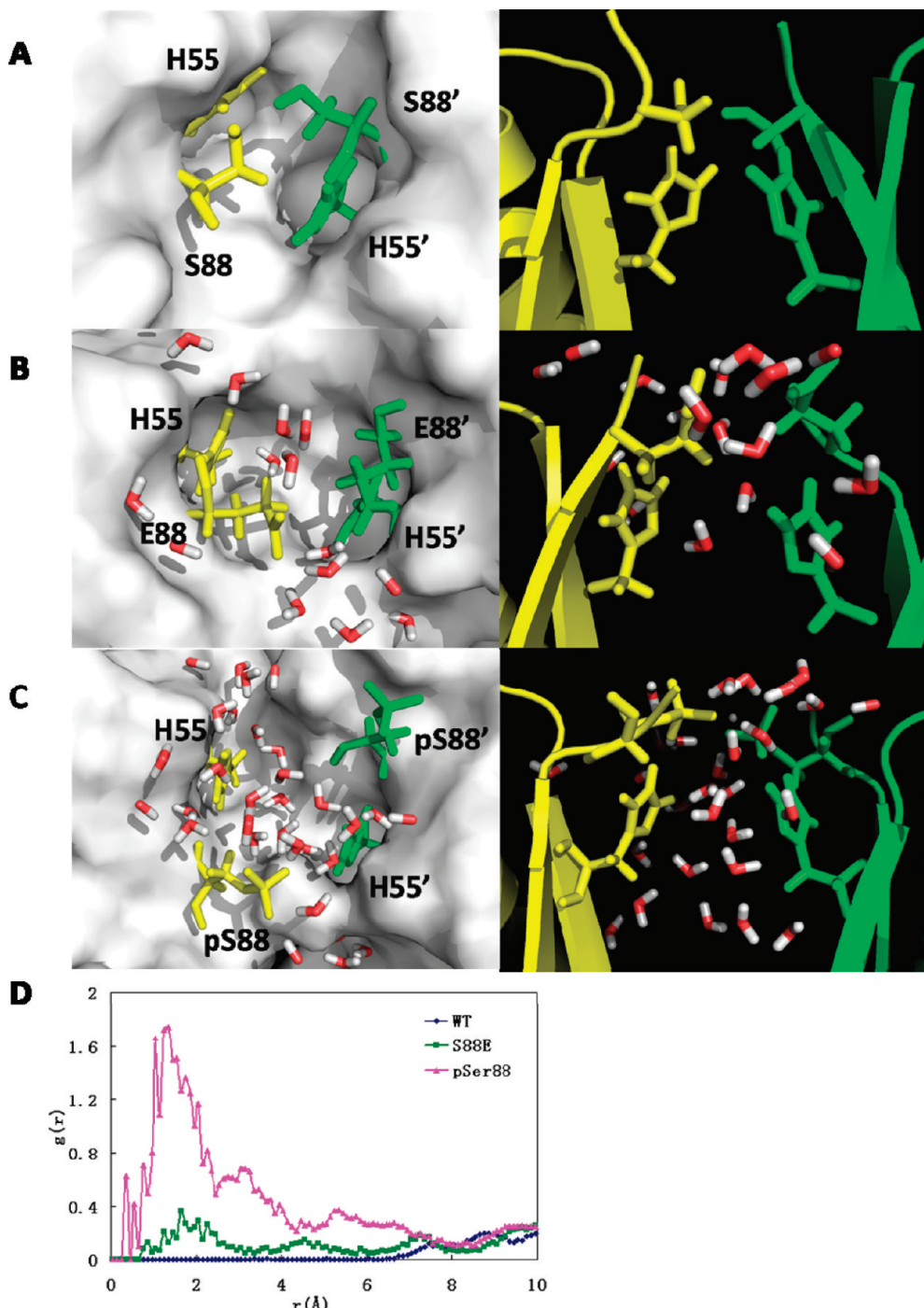


Figure 3. Solvent accessibility of the dimer interface at the C-terminal area. Top and side view snapshots of C-terminal area of WT (A), S88E (B), and pSer88 LC8 (C) at the end of the 50 ns simulation trajectories. Water molecules locating within a distance of 6 Å to His55/His55' are explicitly depicted. The side chains of residue 88 and 55 are shown as sticks. (D) Radial distribution functions (RDF) of water molecules within 10 Å of the C_α atoms of His55/His55' during the last 25 ns in the simulations of WT, S88E, and pSer88 LC8. Details of the RDF calculation are given in the Supporting Information.

H-bonds between Thr67–Trp54' and Lys43–Thr67' were almost removed in pSer88 (Figure 2b). While the **H1** group H-bonds were obviously affected by the mutation/phosphorylation, most of the hydrogen bonds belonging to group **H2** and **H3**, which are further from the C terminus, remained stable during the simulation. The only exception is the H-bonds between Cys56–Tyr65' which were disrupted after 15 ns simulation in pSer88 (Figure 2b).

Upon the opening of the interface at the C-terminus in the S88E and pSer88 systems, some buried residues are exposed

to the solvent. In the wild type LC8, the water molecules are absolutely excluded from the dimer interface around Ser88/Ser88' (Figure 3a). In the S88E and pSer88 LC8, some water molecules entered the dimer interface through the vestibule at E88/pSer88 and penetrated into the interface around His55 (Figure 3b, 3c). This is clearly reflected by the radial distribution function of water molecules around the midpoint between the two C_α atoms of His55 and His55' (Figure 3d). The invasion of water molecules at the dimer interface exposes His55 to the solvent and is expected to disturb the protonation state of His55.

We evaluated the pK_a values of His55/His55' in the end structures of 50 ns simulations of wild type and S88E LC2 dimer by using the PROPKA 2.0 program.^{37,38} The pK_a values increased significantly, from 1.61/0.18 in wild type protein to 3.71/5.05 in S88E, respectively. The estimated pK_a values for the wild type protein are much lower than the experimental results.^{25,40} This discrepancy is usually attributed to the strongly salt-dependent pK_a values in experimental measurement.³⁷

Some water molecules locate between the imidazole rings of His55/His55' and form hydrogen bonds with them. These interactions disrupted the original parallel orientation of the two imidazole rings. The distance between the side chains of His55 and His55' increased from ca. 6 Å in wild type LC8 to ca. 8 Å in both S88E and pSer88 LC8 after 5 ns. Side chain conformational change of His55/His55' affected the hydrogen bonds between His55 and Thr67' and thereby disturbed the hydrogen bond network in the **H1** group, which were weakened or disrupted as aforementioned.

Overall, the parallel 50 ns conventional MD simulations of the wild type, S88E, and pSer88 LC8 systems showed a tendency for dimer dissociation upon phosphorylation or mutation on Ser88 at the C-terminal end of LC8. Introduction of negative charged side chains at Ser88 disturbed the interdomain interactions around the C termini, allowing a penetration of solvent molecules into the dimer interface to impair some of the hydrogen bonds that help to assemble the two monomers. However, it is not feasible to monitor the process of dimer dissociation using conventional MD simulation. We resorted to the steered MD simulation method to get more details of the phosphorylation-induced dimer dissociation in the next section.

3.2. Steered Molecular Dynamics Simulations. In the steered molecular dynamics (SMD) simulations of the wild type, S88E, and pSer88 LC8, the initial structures were chosen as the snapshot structures of the 10 ns conventional MD trajectories, respectively. Three trajectories were conducted for each system. Details of these trajectories are given in Table S1, Supporting Information. The following analyses and discussions are based on one representative trajectory for each system.

The force profiles along the SMD trajectories of the three systems are shown in Figure 4a. In all three systems, the applied forces increased almost linearly at the beginning, indicating that the system resisted the external force due to the interaction networks at the dimer interface. After overcoming a maximum, the forces exhibited a steep decrease, ending at a small final value (ca. 200 pN). The peak of the force profile is a turning point, soon after which most of the hydrogen bonds across the dimer interface were disrupted. The maximum of the applied force in the wild type protein (1648 pN) is obviously higher than those of the S88E (1410 pN) and pSer88 (1356 pN) LC8. Also the wild type LC8 took longer time (816 ps) to reach the maximum compared with the other two systems (684 and 651 ps for S88E and pSer88, respectively). These all indicate that the wild type protein has a more stable dimer interface than that of the mutated or phosphorylated LC8.

As mentioned above, most of the interactions responsible for the dimer assembly were disrupted during the period of the force decrease after the system experienced the largest applied force. Comparison of the force profiles during this period among the three systems reveals that the profile of wild type LC8 is steeper and smoother while those of S88E and pSer88 show stepwise characteristics. Further inspection shows that the differences between the force profiles are largely associated with the

arrangements of hydrogen bond interactions at the dimer interface and originate from the perturbations at the C-terminal area.

In the wild type LC8, before the force reached the maximum, only the backbone hydrogen bonds of the **H3** group (Asn61/61'-Asn61'/61) were disrupted at about 550 ps (Figure 4b). These hydrogen bonds locate at the opposite side of the C-terminus. Between 550 to 800 ps, the rest of the hydrogen bonds at the dimer interface remained stable and the applied force kept increasing during this period. Right after 816 ps when the protein experienced the largest external force, two hydrogen bonds of the **H1** group (Lys43'-Thr67 and Thr67'-Trp54) were broken, showing a moderate force decrease in this period. Then after 900 ps, the rest of the H-bonds were disrupted almost altogether, corresponding to the deepest force decrease in the system. The time evolution pattern of the hydrogen bonds in wild type LC8 along the trajectory demonstrates that the **H3** group hydrogen bonds are the first disrupted interactions at the dimer interface while the backbone H-bonds in **H2** are the last ones. Note that the hydrogen bond between Ser88 and Ser88' was sustained until the final period of the dimer dissociation although the bonding strength is moderate compared with those of **H2** group (Figure 4b).

The SMD trajectories of S88E and pSer88 systems, however, show a dissociation pattern different than that of the wild type protein. The most remarkable difference is that the hydrogen bonds of the **H3** group which dissociated at the earliest stage in the wild type protein were disrupted last in S88E and pSer88 systems. Instead, the disruption of the hydrogen bond network started from the C-terminal region of **H1** group and propagated step by step to the **H3** group region at the opposite end of the interface. In both systems, the **H1** group hydrogen bonds were already significantly weakened or disrupted during the conventional MD simulation, and the only remaining H-bonds between Thr67 and His55' almost disappeared in pSer88-LC8 and were the first broken interactions in S88E at about 700 ps when the applied force reached its maximum. The next disrupted H-bonds are those between Cys56 and Tyr65'. These H-bonds broke around 800 ps in S88E and around 700 ps in pSer88-LC8 corresponding to the maximal external force. The succeeding H-bond dissociation occurred between Val58 and Gly63', at about 930 ps in S88E and 840 ps in pSer88. The hydrogen bond between Asn61 and Asn61' is the last disrupted interaction across the dimer interface.

Overall, the SMD simulations demonstrated that the dimer dissociation is easier for the mutant and the phosphorylated protein than that of the wild type LC8 as expected. Furthermore, the dissociation order of the interdomain interactions is also changed due to the mutation or phosphorylation at Ser88. Note, however, that although the steered MD method allows us to explore the slow conformational transition (μ s to ms) during the computationally accessible time scale, it can at most generate a qualitatively correct pathway for the dimer dissociation, and the relative dissociation progress is not necessarily proportional to actual time.

3.3. Free Energy Calculations. To evaluate the perturbation from the mutation/phosphorylation of Ser88 on the stability of the dimer assembly, we performed the free energy perturbation (FEP) calculation to compare the free energy changes of dimer dissociation between wild type and S88E/pSer88 LC8. Direct estimation of the free energy difference of the dissociation/association process of LC8 is far beyond the scope of all-atom MD simulations. Previous NMR studies of S88E LC2 demonstrated that monomeric and dimeric forms of S88E are in

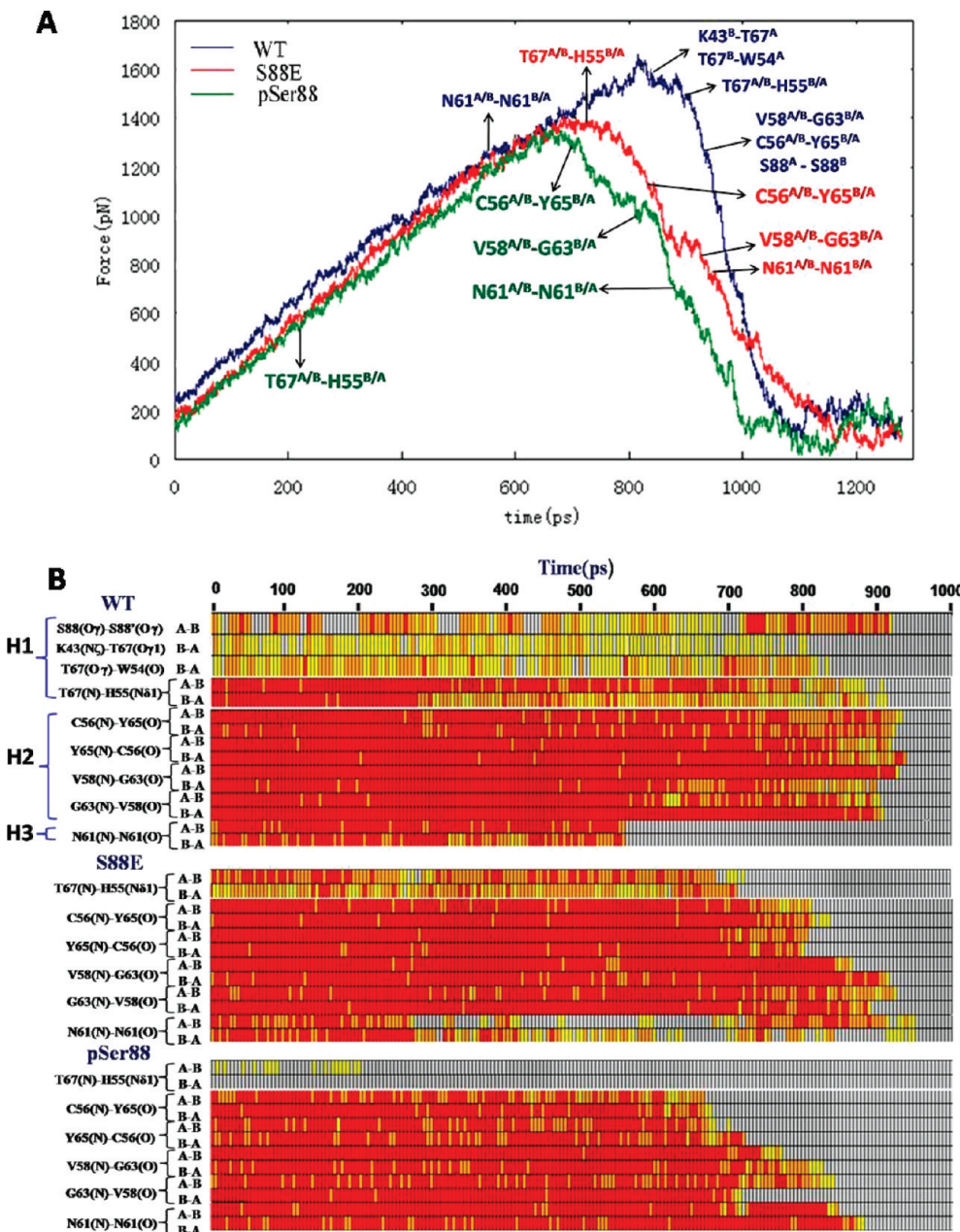


Figure 4. (A) Force profiles of the SMD simulations for WT (blue), S88E (red), and pSer88 (green) LC8. The time of interdomain hydrogen bond breaking along the trajectories are indicated. (B) Variation of interdomain hydrogen bonds along the SMD trajectories in WT, S88E, and pSer88 LC8. The meaning of the diagram is the same as that in Figure 2.

equilibrium, which is concentration dependent. On the basis of this fact, the dissociation problem can be approached by simulating the mutation process of Ser88, i.e., the thermodynamic cycle was designed to calculate the free energy change difference through so-called “alchemical transformation” on Ser88 to Glu88 or pSer88 in the dimeric and monomeric LC8, respectively (Scheme 1). The convergence of FEP calculations was satisfied by checking the overlap of the configurational ensembles of contiguous intermediate states³⁹ (Figure 5). The S88E “alchemical transformations” yielded negative free energy changes of -404.4 and -408.6 kcal/mol in dimeric and monomeric LC8 systems, respectively (Table 1). The free energy changes of “reverse” transformation from Glu88 to Ser88 were also calculated, yielding values of 410.0 and 418.9 kcal/mol, respectively. Apparently, there is an “asymmetry” in the FEP calculation. This asymmetry is more evident in the phosphorylation transformation. Following a widely used “direct averaging” method, we simply took the mean ($\Delta\bar{G}_1$ and $\Delta\bar{G}_2$) of the forward and reverse results as an estimate of the free energy changes of the alchemical transformations, i.e.,

$$\begin{aligned}\Delta\bar{G}_1 &= (\Delta G_1 - \Delta G'_1)/2 \\ \Delta\bar{G}_2 &= (\Delta G_2 - \Delta G'_2)/2 \\ \Delta\Delta G^{\text{dissoc}} &= \Delta G_2^{\text{dissoc}} - \Delta G_1^{\text{dissoc}} = \Delta\bar{G}_2 - \Delta\bar{G}_1\end{aligned}$$

where the subscripts 1 and 2 denote the dimer and the monomer, respectively.

Thus, calculated $\Delta\Delta G^{\text{dissoc}}$ for S88E and pSer88 are -6.6 ± 4.5 and -50.8 ± 7.0 kcal/mol, respectively. These values give a rough estimate of the relative stability of the dimer assembly between the wild type protein and the S88E/pSer88 LC8.

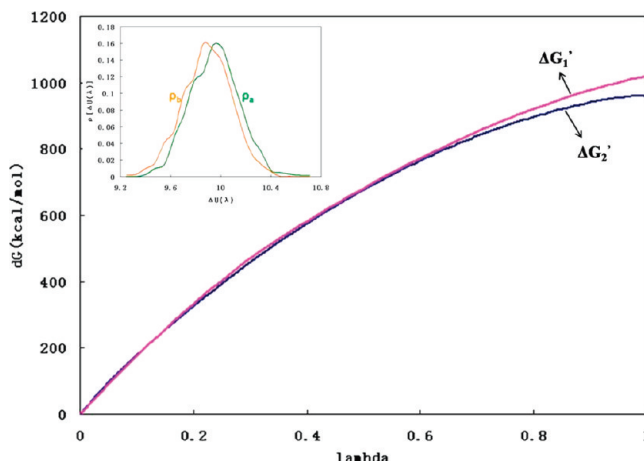
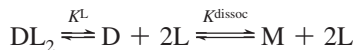


Figure 5. Evolution of the Gibbs free energy as a function of the coupling parameter λ in the transformation from WT to pSer88 LC8 dimer. Inset: Overlapping configurational ensembles (embodied in the density of states $\rho[\Delta U(x)]$) of contiguous intermediate states at $\lambda = 0.5$. $\rho[\Delta U(x)]$ was calculated as described in ref 39.

Phosphorylation or mutation at Ser88 obviously destabilizes the dimer association, in agreement with the experimental observations. The $\Delta\Delta G^{\text{dissoc}}$ due to the S88E mutation is in good agreement with the experimentally determined value of -8.1 kcal/mol.²⁵ Our calculation predicts that the effect of phosphorylation (-50.8 ± 7.0 kcal/mol) on the dimer stability is much more prominent than that of S88E mutation. We also observed the penetration of water molecules into the dimer interface in the alchemical transformations. This is consistent with the 50 ns simulation. The results of the free energy decomposition analysis showed that most of the free energy changes come from electrostatic interactions, while the contribution from the van der Waals interaction is minor (Table 1). This is also in agreement with the experimental analysis.²⁵ The electrostatic contributions include the solvation of the negative charges on mutated/phosphorylated Ser88 and the like-charge repulsion between E88/E'88 or pS88/pS88'.

We also evaluated the perturbation from the phosphomimetic mutation of Ser88 on the dimer assembly in the presence of Swa peptide. Under the assumption of the following reaction:

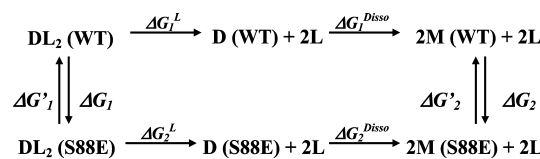


the thermodynamic cycle can be designed as shown in Scheme 2. It follows that,

$$\Delta\Delta G = \Delta\bar{G}_2 - \Delta\bar{G}_1 = \Delta G_2^L - \Delta G_1^L + \Delta G_2^{\text{dissoc}} - \Delta G_1^{\text{dissoc}}$$

i.e., in the presence of bound ligand, the calculated $\Delta\Delta G$ can be decomposed into the effect of mutation on the ligand binding

SCHEME 2: Thermodynamic Cycle Used To Calculate the Difference of Dimer Dissociation Free Energy Change between Wild Type and S88E/pSer88 LC8 in the Presence of Bound Ligands (see text for more details)



and that on the dimer assembly. The calculated $\Delta\Delta G$ for S88E/Swa is -7.9 ± 5.2 kcal/mol (Table 1). Compared with the $\Delta\Delta G^{\text{dissoc}}$ for S88E (-6.6 ± 4.5 kcal/mol), it gives the perturbation from mutation on ligand binding of -1.3 kcal/mol. However, considering the error bar of the calculation, we suggest that the effect of phosphomimetic mutation on the ligand-bound LC8 dimer is primarily to promote the dimer dissociation.

4. Discussion

The dimer assembly of LC8 can be modulated by phosphorylation of Ser88 at the interface. Our simulation results provide an atomic picture of the destabilization mechanism. Although the 50 ns conventional MD simulations did not demonstrate large scale conformational change of LC8 dimer upon phosphorylation or phosphomimetic mutation at Ser88, it did provide evidence of local structural perturbation around Ser88. The mutation/phosphorylation-induced hydrogen bond disruption and like-charge repulsion between the two Ser88 increases the inter-residue distance. The slight separation of Ser88 upon phosphorylation or mutation gives rise to an entrance of water molecules into the dimer interface. The simulation trajectories showed that the penetrated water molecules perturb the interfacial hydrogen bond network around His55 by coordinating with the side chain of His55. Note that in our simulation neither His55 is protonated, corresponding to the most tightly dimerization form of LC8. It is well-known that the pH-dependent LC8 dimer–monomer transformation is attributed to the protonation of His55.⁴⁰ The penetration of water molecules into the dimer interface observed in our simulation raises the pK_a value of His55/His55' and thereby its protonation ratio, destabilizing the dimer. Therefore, in this respect the dimer assembly regulation by phosphorylation of Ser88 can be considered as an indirect modulation of His55 protonation state.

The SMD simulation results provide further evidence showing that mutation/phosphorylation weakens the dimer association. In addition, SMD simulations reflect the relative strengths of interactions across the dimer interface and demonstrated different dissociation patterns between wild type and S88E/pSer88 LC8. In wild type LC8, the main chain hydrogen bonds of the **H2** group at the middle of the interface represents the most stable interactions, helping to form the antiparallel β -sheets between the two monomers. The **H1** group hydrogen bonds involving side chains are much weaker than the **H2** group. This can also be seen in the 10 ns conventional MD simulations, along the trajectories of which the percentage of emergence of

TABLE 1: Free Energy Differences (kcal/mol) Calculated Using the FEP Method^a

	ΔG_1	$\Delta G'_1$	$\Delta\bar{G}_1$	ΔG_2	$\Delta G'_2$	$\Delta\bar{G}_2$	$\Delta\Delta G^{\text{dissoc}}$	$\Delta\Delta\bar{G}_{\text{elec}}$	$\Delta\Delta\bar{G}_{\text{vdw}}$
S88E	-404.4 ± 3.6	410.0 ± 3.6	-407.2 ± 2.5	-408.6 ± 5.4	418.9 ± 5.4	-413.8 ± 3.8	-6.6 ± 4.5	-5.6	-0.7
pSer88	-885.0 ± 5.9	951.4 ± 5.2	-918.2 ± 3.9	-929.4 ± 9.2	1008.9 ± 7.0	-969.0 ± 5.8	-50.9 ± 7.0	-60.5	8.8
S88E/Swa	-391.7 ± 4.7	420.0 ± 5.1	-405.9 ± 3.5	-408.6 ± 5.4	418.9 ± 5.4	-413.8 ± 3.8	-7.9 ± 5.2	-23.2	15.6

^a $\Delta\Delta\bar{G}_{\text{elec}}$ and $\Delta\Delta\bar{G}_{\text{vdw}}$ represent the electrostatic and van der Waals contributions to $\Delta\Delta G^{\text{dissoc}}$, respectively.

the **H1** group hydrogen bonds is relatively lower. In the SMD simulations, however, upon the external pulling force, the **H1** group H-bonds were not broken initially. They last longer than the hydrogen bonds of the **H3** group at the opposite end of the interface. In contrast, in the S88E/pSer88 LC8 H-bonds of the **H1** group were the first disrupted interactions, and the **H3** group H-bond seems to be strengthened by the phosphorylation and last even longer than that of the **H2** group. Therefore, in the wild type LC8, the **H3** group H-bond represents the soft spot of the interface, while the phosphorylation at Ser88 makes the C-terminal end the weakest point.

The free energy calculations gave a quantitative measurement of the destabilization of the dimer induced by phosphomimetic mutation or phosphorylation at Ser88. The calculated $\Delta\Delta G^{\text{dissoc}}$ for S88E of -6.6 kcal/mol is in good agreement with the experimental results. It should be noted that in our calculation, both Glu88 are deprotonated and the value of $\Delta\Delta G^{\text{dissoc}}$ represents an upper limit of the destabilization effect. Similarly, both Ser88 are phosphorylated and each phosphoserine bears two negative charges in the simulation. Thus, the calculated $\Delta\Delta G^{\text{dissoc}}$ of -50.8 kcal/mol is also expected to be the upper limit of the destabilization free energy. Although the decomposition of the calculated free energy differences is not exact due to the neglect of the coupling terms,⁴¹ the results can still reflect that the destabilization effect of phosphorylation on dimer assembly mainly originates from electrostatic repulsion between the two negatively charged phosphoserines. Note that in the free energy calculation, both His55 were deprotonated. Therefore, the calculated destabilization energy does not include the contribution from the protonation state change of His55, which was shown to couple with the phosphorylation/mutation on Ser88 in the above discussion.

5. Conclusion

In summary, the MD simulations and free energy calculations in this study provide the detailed mechanisms of the phosphorylation-regulated LC8 dimer dissociation. It is found that the phosphorylation at Ser88 not only disturbs the interdomain hydrogen bond interactions but also affects the protonation state of His55. The free energy calculations gave the quantitative destabilization effect of phosphomimetic mutation/phosphorylation on the dimer assembly and reveal that the destabilization effect mainly originates from the electrostatic interactions.

Acknowledgment. This work was supported by National High Technology Research Program of China (2006AA02A320), National Major Basic Research Program of China (2009CB918600, 2011CB808505), National Science Foundation of China (20973040, 31070642), Science & Technology Commission of Shanghai Municipality (08DZ2270500), and Shanghai Leading Academic Discipline Project (B108). We are grateful to the Shanghai Supercomputer Center and Computer Center of Fudan University for their allocation of computer time.

Supporting Information Available: A table of the details of all SMD trajectories, and the equation we used to calculate the radial distribution function of water molecules in Figure 3 D. This material is available free of charge via the Internet at <http://pubs.acs.org>.

References and Notes

- Piperno, G.; Luck, D. J. L. Axonemal Adenosine Triphosphatases from Flagella of Chlamydomonas-Reinhardtii - Purification of 2 Dyneins. *J. Biol. Chem.* **1979**, 254, 3084–3090.
- Dick, T.; Ray, K.; Salz, H. K.; Chia, W. Cytoplasmic dynein (ddlc1) mutations cause morphogenetic defects and apoptotic cell death in *Drosophila melanogaster*. *Mol. Cell. Biol.* **1996**, 16, 1966–1977.
- Lo, K. W. H.; Kan, H. M.; Pfister, K. K. Identification of a novel region of the cytoplasmic dynein intermediate chain important for dimerization in the absence of the light chains. *J. Biol. Chem.* **2006**, 281, 9552–9559.
- Benashski, S. E.; Harrison, A.; PatelKing, R. S.; King, S. M. Dimerization of the highly conserved light chain shared by dynein and myosin V. *J. Biol. Chem.* **1997**, 272, 20929–20935.
- Vallee, R. B.; Williams, J. C.; Varma, D.; Barnhart, L. E. Dynein: An ancient motor protein involved in multiple modes of transport. *J. Neurobiol.* **2004**, 58, 189–200.
- Espindola, F. S.; Suter, D. M.; Partata, L. B. E.; Cao, T.; Wolenski, J. S.; Cheney, R. E.; King, S. M.; Mooseker, M. S. The light chain composition of chicken brain myosin-Va: Calmodulin, myosin-II essential light chains, and 8-kDa dynein light chain/PIN. *Cell. Motil. Cytoskeleton* **2000**, 47, 269–281.
- Makokha, M.; Hare, M.; Li, M. G.; Hays, T.; Barbar, E. Interactions of cytoplasmic dynein light chains Tctex-1 and LC8 with the intermediate chain IC74. *Biochemistry* **2002**, 41, 4302–4311.
- Lo, K. W. H.; Naisbitt, S.; Fan, J. S.; Sheng, M.; Zhang, M. J. The 8-kDa dynein light chain binds to its targets via a conserved (K/R)XTQT motif. *J. Biol. Chem.* **2001**, 276, 14059–14066.
- King, S. M.; Barbarese, E.; Dillman, J. F.; PatelKing, R. S.; Carson, J. H.; Pfister, K. K. Brain cytoplasmic and flagellar outer arm dyneins share a highly conserved M(r) 8,000 light chain. *J. Biol. Chem.* **1996**, 271, 19358–19366.
- Jaffrey, S. R.; Snyder, S. H. PIN. An associated protein inhibitor of neuronal nitric oxide synthase. *Science* **1996**, 274, 774–777.
- Crepieux, P.; Kwon, H.; Leclerc, N.; Spencer, W.; Richard, S.; Lin, R. T.; Hiscott, J. I kappa B alpha physically interacts with a cytoskeleton-associated protein through its signal response domain. *Mol. Cell Biol.* **1997**, 17, 7375–7385.
- Puthalakath, H.; Huang, D. C. S.; O'Reilly, L. A.; King, S. M.; Strasser, A. The proapoptotic activity of the Bcl-2 family member Bim is regulated by interaction with the dynein motor complex. *Mol. Cell* **1999**, 3, 287–296.
- Vadlamudi, R. K.; Bagheri-Yarmand, R.; Yang, Z.; Balasenthil, S.; Nguyen, D.; Sahin, A. A.; den Hollander, P.; Kumar, R. Dynein light chain 1, a p21-activated kinase 1-interacting substrate, promotes cancerous phenotypes. *Cancer Cell* **2004**, 5, 575–585.
- Lo, K. W. H.; Kan, H. M.; Chan, L. N.; Xu, W. G.; Wang, K. P.; Wu, Z. G.; Sheng, M.; Zhang, M. J. The 8-kDa dynein light chain binds to p53-binding protein 1 and mediates DNA damage-induced p53 nuclear accumulation. *J. Biol. Chem.* **2005**, 280, 8172–8179.
- King, S. M.; PatelKing, R. S. The M(R)=8,000 and 11,000 Outer Arm Dynein Light-Chains from Chlamydomonas Flagella Have Cytoplasmic Homologs. *J. Biol. Chem.* **1995**, 270, 11445–11452.
- Liang, J.; Jaffrey, S. R.; Guo, W.; Snyder, S. H.; Clardy, J. Structure of the PIN/LC8 dimer with a bound peptide. *Nat. Struct. Biol.* **1999**, 6, 735–740.
- Fan, J. S.; Zhang, Q.; Tochio, H.; Li, M.; Zhang, M. J. Structural basis of diverse sequence-dependent target recognition by the 8 kDa dynein light chain. *J. Mol. Biol.* **2001**, 306, 97–108.
- Barbar, E.; Kleinman, B.; Imhoff, D.; Li, M. G.; Hays, T. S.; Hare, M. Dimerization and folding of LC8, a highly conserved light chain of cytoplasmic dynein. *Biochemistry* **2001**, 40, 1596–1605.
- Mohan, P. M. K.; Barve, M.; Chatterjee, A.; Hosur, R. V. PH driven conformational dynamics and dimer-to-monomer transition in DLC8. *Protein Sci.* **2006**, 15, 335–342.
- Wang, W. N.; Lo, K. W. H.; Kan, H. M.; Fan, J. S.; Zhang, M. J. Structure of the monomeric 8-kDa dynein light chain and mechanism of the domain-swapped dimer assembly. *J. Biol. Chem.* **2003**, 278, 41491–41499.
- Makokha, M.; Huang, Y. P. J.; Montelione, G.; Edison, A. S.; Barbar, E. The solution structure of the pH-induced monomer of dynein light-chain LC8 from *Drosophila*. *Protein Sci.* **2004**, 13, 727–734.
- Song, C. Y.; Wen, W. Y.; Rayala, S. K.; Chen, M. Z.; Ma, J. P.; Zhang, M. J.; Kumar, R. Serine 88 phosphorylation of the 8-kDa dynein light chain 1 is a molecular switch for its dimerization status and functions. *J. Biol. Chem.* **2008**, 283, 4004–4013.
- Lightcap, C. M.; Sun, S.; Lear, J. D.; Rodeck, U.; Polenova, T.; Williams, J. C. Biochemical and structural characterization of the Pak1-LC8 interaction. *J. Biol. Chem.* **2008**, 283, 27314–27324.
- Song, Y. J.; Benison, G.; Nyarko, A.; Hays, T. S.; Barbar, E. Potential role for phosphorylation in differential regulation of the assembly of dynein light chains. *J. Biol. Chem.* **2007**, 282, 17272–17279.
- Benison, G.; Chiodo, M.; Karplus, P. A.; Barbar, E. Structural, Thermodynamic, and Kinetic Effects of a Phosphomimetic Mutation in Dynein Light Chain LC8. *Biochemistry* **2009**, 48, 11381–11389.

- (26) Phillips, J. C.; Braun, R.; Wang, W.; Gumbart, J.; Tajkhorshid, E.; Villa, E.; Chipot, C.; Skeel, R. D.; Kazle, L.; Schulten, K. Scalable molecular dynamics with NAMD. *J. Comput. Chem.* **2005**, *26*, 1781–1802.
- (27) MacKerell, A. D.; Feig, M.; Brooks, C. L. Improved treatment of the protein backbone in empirical force fields. *J. Am. Chem. Soc.* **2004**, *126*, 698–699.
- (28) Jorgensen, W. L.; Chandrasekhar, J.; Madura, J. D.; Impey, R. W.; Klein, M. L. Comparison of Simple Potential Functions for Simulating Liquid Water. *J. Biol. Chem.* **1983**, *79*, 926–935.
- (29) Martyna, G. J.; Tobias, D. J.; Klein, M. L. Constant-Pressure Molecular-Dynamics Algorithms. *J. Chem. Phys.* **1994**, *101*, 4177–4189.
- (30) Feller, S. E.; Zhang, Y. H.; Pastor, R. W.; Brooks, B. R. Constant-Pressure Molecular-Dynamics Simulation - the Langevin Piston Method. *J. Chem. Phys.* **1995**, *103*, 4613–4621.
- (31) Darden, T.; York, D.; Pedersen, L. Particle Mesh Ewald - an N.Log(N) Method for Ewald Sums in Large Systems. *J. Chem. Phys.* **1993**, *98*, 10089–10092.
- (32) Darden, T.; Perera, L.; Li, L. P.; Pedersen, L. New tricks for modelers from the crystallography toolkit: the particle mesh Ewald algorithm and its use in nucleic acid simulations. *Struct. Fold. Des.* **1999**, *7*, R55–R60.
- (33) Ryckaert, J. P.; Cicotti, G.; Berendsen, H. J. C. Numerical-Integration of Cartesian Equations of Motion of a System with Constraints - Molecular-Dynamics of N-Alkanes. *J. Comput. Phys.* **1977**, *23*, 327–341.
- (34) Pearlman, D. A. A Comparison of Alternative Approaches to Free-Energy Calculations. *J. Phys. Chem.* **1994**, *98*, 1487–1493.
- (35) Zwanzig, R. W. High-Temperature Equation of State by a Perturbation Method I. Nonpolar Gases. *J. Chem. Phys.* **1954**, *22*, 1420–1426.
- (36) Benison, G.; Karplus, P. A.; Barbar, E. Structure and dynamics of LC8 complexes with KXTOT-motif peptides: Swallow and dynein intermediate chain compete for a common site. *J. Mol. Biol.* **2007**, *371*, 457–468.
- (37) Li, H.; Robertson, A. D.; Jensen, J. H. Very fast empirical prediction and rationalization of protein pK(a) values. *Proteins* **2005**, *61*, 704–721.
- (38) Bas, D. C.; Rogers, D. M.; Jensen, J. H. Very fast prediction and rationalization of pK(a) values for protein-ligand complexes. *Proteins* **2008**, *73*, 765–783.
- (39) Chipot, C. Milestones in the Activation of a G Protein-Coupled Receptor. Insights from Molecular-Dynamics Simulations into the Human Cholecystokinin Receptor-1. *J. Chem. Theory Comput.* **2008**, *4*, 2150–2159.
- (40) Nyarko, A.; Cochrun, L.; Norwood, S.; Pursifull, N.; Voth, A.; Barbar, E. Ionization of His 55 at the dimer interface of dynein light-chain LC8 is coupled to dimer dissociation. *Biochemistry* **2005**, *44*, 14248–14255.
- (41) Free Energy Calculations. *Theory and applications in chemistry and biology*; Chipot, C., Pohorille, A., Eds.; Springer-Verlag: New York, 2007; p 69.

JP1048869